Letters in Applied NanoBioScience
Open-Access Journal (ISSN: 2284-6808)

Article
Volume 14, Issue 1, 2025, 2
https://doi.org/10.33263/LIANBS141.002

Exploring Small Molecules as Novel Drug Candidates Targeting 4-Hydroxy-Tetrahydrodipicolinate Reductase in *Mycobacterium tuberculosis*: Insights from Molecular Dynamics Simulation and Principal Component Analysis

Rehman Ajijur [1], Khan Mohammad Kalim Ahmad [2,*]

[1] Department of Bioinformatics NIMS Institute of Allied Medical Science and Technology, NIMS University, Jaipur-303121, Rajasthan, India
[2] Department of Bioengineering, Integral University, Lucknow-226026, Uttar Pradesh, India
* Correspondence: mkakhan@iul.ac.in;

Scopus Author ID 57193235237
Received: 12.05.2024; Accepted: 7.07.2024; Published: 21.09.2024

Abstract: 4-hydroxy-tetrahydrodipicolinate reductase (DapB) is a vital enzyme present in bacteria, primarily *Mycobacterium tuberculosis*, and plays a pivotal role in the biosynthesis of diaminopimelic acid (DAP), an essential component of the bacterial cell wall. Inhibition of DapB disrupts DAP synthesis, leading to structural damage to the bacterial cell wall, making the bacterium more susceptible to the host immune response, and enhancing the effectiveness of existing anti-TB treatments. DapB is absent in human cells, which makes it a suitable pharmacological target. This study utilized advanced computational techniques, including structure-based virtual screening (SBVS), ADMET profiling, molecular docking, dynamic simulations, and principal component analysis, to identify small molecules from the vast digital library of the MCULE database that selectively inhibits DapB as a strategy to combat tuberculosis, a significant global health challenge. The proposed research identified MCULE-9296301908-0-1, with a computed binding energy (ΔG) of -9.9 kcal/mol, as a promising candidate for an anti-tubercular drug. Notably, this compound surpassed the binding affinity of a known potential inhibitor, 2,6-Pyridinedicarboxylic acid (PDC) (-7.5 kcal/mol). However, research findings depend on computational methods, and rigorous laboratory experiments are necessary for validation. This study represents a significant step toward the fight against tuberculosis drug resistance.

Keywords: DAP/lysine pathway; *Mycobacterium tuberculosis*; DapB; PDC; SBVS; docking; MD simulation; PCA.

1. Introduction

Tuberculosis (TB), a severe and highly contagious disease caused by *Mycobacterium tuberculosis*, can affect not only the lungs but also various other organs, including extrapulmonary TB [1,2]. Despite its discovery over a century ago, a dependable TB vaccine remains elusive. Although the BCG vaccine provides limited protection, recent studies on macaques suggest that intravenous BCG vaccination can trigger a robust immune response, offering substantial protection against future *Mycobacterium tuberculosis* infections [3]. Identifying TB requires differentiating between active TB (ATB) and latent TB (LTBI). Current immunological methods, such as the Mantoux Tuberculin skin test and interferon-gamma release assays, are not consistently reliable in distinguishing ATB from LTBI. Testing

and treating LTBI is recommended for high-risk individuals to reduce the likelihood of ATB. Advanced molecular tests, such as the GeneXpert nucleic acid-based test, are gradually replacing conventional methods for diagnosing ATB, such as sputum acid-fast bacillus staining. TB treatment requires a long-term, multiple-drug regimen [4,5]. The emergence of drug-resistant TB, particularly multidrug-resistant (MDR) and extensively drug-resistant (XDR) TB, poses a significant challenge. Ongoing research is essential to understand the relationship between the host and pathogen and to develop effective treatments [6–9]. Particular attention should be paid to drug-resistant strains to ensure that new therapies do not contribute to their emergence and spread.

Biosynthesis of diaminopimelic acid (DAP) and lysine is a critical metabolic process in bacteria, mainly *Mycobacterium tuberculosis*. This pathway is essential for synthesizing two vital components of the bacterial cell wall: diaminopimelic acid and lysine. The biosynthesis of DAP and lysine begins with the conversion of aspartate to diaminopimelate, a process catalyzed by aspartate kinase and several other enzymatic reactions. The final step in this pathway involves the synthesis of meso-diaminopimelate (DAP), which serves as a crucial building block for peptidoglycan synthesis, a vital component of the bacterial cell wall [10,11].

In *Mycobacterium tuberculosis*, the biosynthesis of lysine from DAP is a branch point where the organism can decide to continue the pathway to produce lysine or divert intermediates to other metabolic pathways. Lysine synthesis involves additional enzymatic steps, and incorporating DAP into the peptidoglycan layer of the bacterial cell wall provides structural integrity and protection against osmotic stress [12,13]. This pathway is an attractive target for antimicrobial drug development because it maintains bacterial cell wall integrity.

In the intricate domain of bacterial metabolism, 4-hydroxy-tetrahydrodipicolinate reductase (DapB) is pivotal in lysine production, an indispensable amino acid. DapB attaches to the substrate 4-hydroxy-tetrahydrodipicolinate (HTPA) at its active site, with NAD(P)H as a cofactor, facilitating the necessary reducing equivalents for the catalytic process. This process entails the reduction of HTPA to tetrahydrodipicolinate (THPA), with hydride ions (H-) transferred from the cofactor (NAD(P)H) to the substrate. The final result was the conversion of HTPA and NAD(P)H to THPA and NAD(P)+, respectively. Subsequently, DapB releases the reduced product, THPA, from its active site [12–14]. The oxidized cofactor (NAD(P)+) is then restored to NAD(P)H through cellular redox processes, allowing DapB to participate in another round of the catalytic cycle. Understanding the precise molecular mechanisms of enzymes, such as DapB, is crucial for designing targeted inhibitors. Small molecules that can bind to the active site of DapB and impede substrate binding or catalytic activity are promising drug candidates for inhibiting bacterial growth. The specifics of the mechanism and structure of DapB in *Mycobacterium tuberculosis* are critical considerations for developing selective and efficacious inhibitors for therapeutic purposes.

Biosynthetic pathways involving DAP and lysine are currently the focus of extensive research in anti-TB drug discovery. The enzyme 4-hydroxy-tetrahydrodipicolinate reductase (DapB) is considered a crucial therapeutic target in this pathway, and the development of small-molecule inhibitors against it holds great promise for preventing tuberculosis [12,14–17]. As part of a proposed research initiative, potential investigational ligands against DapB were identified using Pfizer's Lipinski rule and virtual screening, followed by a comprehensive analysis of the MCULE digital library. Compounds that passed the BOILED-egg test, which includes HIA and BBB permeability assessments using TPSA and WLOGP, underwent drug-likeness and PAINS screening [18,19]. The stability of the top ligands was assessed using MD

simulations and the parameters above. A meticulous comparative analysis was conducted between the top lead and control molecules to identify potential antitubercular drug candidates. This systematic approach holds great promise for advancing anti-TB drug discovery efforts.

2. Materials and Methods

2.1. 3D structure retrieval and energy minimization of protein.

We obtained the three-dimensional crystal structure of DapB from *Mycobacterium* in complex with NADPH and 2,6 pyridine dicarboxylic acid (5TJZ) from the RCSB Protein Data Bank (PDB) database, with a resolution of 1.50 Å [20]. To generate a suitable three-dimensional input file for the chosen docking tool, we isolated only the apo-form of the protein, excluding other components, such as heteroatoms, ions, and additional molecules. To improve the conformation and structural integrity of the target protein, we conducted an energy minimization process using the SwissPDB viewer. This involves optimizing the protein structure by minimizing unfavorable interactions and stabilizing the molecule, resulting in a more accurate representation of the protein's native state for subsequent computational analyses [21–24].

2.2. Virtual screening using structural approaches for precision drug discovery.

For target-based virtual screening, we employed the internet-based drug discovery resource site MCULE, which hosts an extensive digital collection of over five million purchasable and synthetically accessible ligands. Employing a structure-based virtual screening (SBVS) method, we adhered to Pfizer's rule of five (RO5), a set of specific criteria, including a molecular weight (MW) of 500 Da or less, a limited number of hydrogen bond donors (HBD $\leq$ 5), a restricted number of hydrogen bond acceptors (HBA $\leq$ 10), and a partition coefficient (LogP) of 5 or less, to filter small molecules [25]. To ensure a diverse range of compounds, we set the sample size to 1000 and established a resemblance search threshold of 0.90 for the input query. Utilizing the FP2 fingerprint in Open Babel as a 2D search algorithm, we conducted the SBVS workflow while maintaining the remaining search parameters at their default settings to thoroughly investigate potential ligands that met the specified criteria [26].

2.3. Retrieval of three-dimensional structures for the reference molecule 2,6-pyridine dicarboxylic acid (PDC).

Two-dimensional structures of PDC were obtained from the NCBI PubChem database and converted into corresponding three-dimensional structures using the Accelrys Discovery Studio Visualizer (DSV) [27]. This process involves the precise translation of chemical structures into three-dimensional conformations. Energy minimization was performed using the same protocol as for the receptor molecule to ensure structural integrity and optimize the conformation of the inhibitors. This step aimed to refine and stabilize the 3D structure of the PDC by aligning their conformations for further computational analyses and modeling [28–30].

2.4. Employing AutoDock Vina for docking simulation.

The use of the MCULE online drug discovery platform, which incorporates AutoDock Vina, enabled the execution of molecular docking simulations of DapB and SBVS ligands. To

begin these simulations, a three-dimensional protein input file in PDB format was submitted to the AutoDock Vina interface and made available on the MCULE portal. To ensure the precision of the docking results, a grid size was established to encompass the specific binding pocket of the protein [31,32]. Docking parameters, such as the number of binding modes per ligand and exhaustiveness, were maintained at their default settings. Notably, the critical criterion for evaluating the best pose of ligand hits within the binding site of DapB is the free energy of binding (ΔG). This metric is essential for identifying and ranking the most favorable interactions between ligands and the binding crevice of the protein, providing valuable insights into potential binding affinities and orientations [33,34].

2.5. Assessing potentially harmful moieties in screened ligands.

Through extensive research using the toxicity checker integrated within the MCULE resource portal, the primary objective was to identify and scrutinize hazardous components, including moieties, fragments, and substructures, present within ligand hits obtained through virtual screening. This assessment utilized the SMARTS algorithm, which guarantees meticulous examination to detect any chemical elements in the screened ligands that could pose potential risks to human health or the environment. The use of this advanced algorithm significantly enhances the accuracy and reliability of the evaluation, thereby providing crucial information on the safety profile of the identified ligands [25].

2.6. Evaluating human intestinal absorption (HIA) and blood-brain barrier (BBB) permeation using the BOILED-Egg model.

The SwissADME tool was used to evaluate the potential of the predicted ligands for human intestinal absorption (HIA) and blood-brain barrier (BBB) permeation using the BOILED-egg model. This model, also known as the Egan Egg model, employs two key physicochemical features: WLOGP with a reference value of ≤ 5.88 to assess lipophilicity and TPSA with a reference value of ≤ 131.6 $Å^2$ to evaluate apparent polarity. The BOILED-Egg model offers a visual representation that illustrates how much a molecule deviates from the optimal characteristics required for efficient absorption into the human body. By providing insights into a molecule's lipophilicity and apparent polarity, this model aids in determining its suitability for effective absorption and permeation across the blood-brain barrier. This visual representation is a valuable tool that offers a nuanced understanding of a molecule's potential for optimal uptake and permeation [35–38].

2.7. Assessing medicinal chemistry attributes.

Evaluating medicinal chemical properties requires identifying promising compounds, often referred to as frequent hitters. This process was facilitated by using the Pan Assay Interference Structure (PAINS) alert option in the SwissADME tools. Specifically, the Ruth Brenk alert was used to detect undesirable substructures, dyes, and toxic moieties. This approach aims to identify elements within compounds that could potentially interfere with assays or possess characteristics deemed unfavorable for medicinal chemistry applications. The strategic use of the PAINS alert option enhances the screening process, contributing to identifying and excluding compounds with potential drawbacks in medicinal chemistry [39,40].

2.8. Assessing stability via molecular dynamics simulation.

A series of computational simulations utilizing GROMACS 5.1.2 at the molecular mechanics (MM) level, with a temperature of 300 K, to assess the stability of the optimal ligand-DapB complex and the reference drug PDC-DapB. Employing the gmx grep module, the ligands were extracted from their respective complexes, and the CHARMM general force field (CGenFF) server was used to predict the topology and force field parameter files for the selected ligand hits [41–43]. The pdb2gmx modules of GROMACS 5.1.2 were employed to generate topologies for DapB. All complexes were immersed in a dodecahedron box of water molecules with a 10 Å margin and underwent a minimization phase consisting of 250,000 steps using the steepest descent algorithm. The equilibration phase involved raising the system temperature from 0 K to 300 K over a ten-nanosecond duration under constant NVT (number of particles, volume, and temperature) and NPT (number of particles, pressure, and temperature) conditions. A particle mesh was established using the Ewald method following equilibration. Various GROMACS modules have been utilized to thoroughly analyze the molecular dynamic parameters and assess complexes' structural stability and dynamics [44–46]. This comprehensive computational approach offers valuable insights into the behavior of the ligand-DapB complex and the reference drug PDC-DapB, contributing to a deeper understanding of their potential interactions and stability in a simulated environment.

2.10. Assessing stability via PCA.

To investigate the dynamics and conformational changes occurring within the protein-ligand docking complexes, Principal Component Analysis (PCA) was employed. Using the Galaxy platform, PCA was applied to identify statistically meaningful conformations in the 10 ns trajectory of DapB, the identified ligands, and the control molecule PDC [47].

3. Results and Discussion

3.1. Analysis of ligand suitability through Lipinski rule of five in structure-based virtual screening.

Our analysis of structure-based virtual screening followed the stringent criteria outlined by Pfizer's Lipinski rule of five (RO5), which is widely employed in medicinal chemistry to evaluate the drug-likeness of chemical compounds and their potential oral bioavailability. The RO5 criteria, formulated by Dr. Christopher Lipinski, consist of a molecular weight (MW) of less than 500 Daltons, no more than 10 hydrogen bond acceptor (HBA) groups, no more than 5 hydrogen bond donor (HBD) groups, and a calculated octanol-water partition coefficient (logP) of less than 5. In our screening process, we comprehensively examined the investigational ligands from the MCULE digital repository. Of the initial 40,401,650 hits, 32,404,135 ligands adhered to the Lipinski RO5 criteria, demonstrating significant docking within the DapB-binding pocket. While adherence to the Lipinski RO5 criteria is indicative of favorable pharmacokinetic properties, it is important to note that compliance with these guidelines is not an absolute requirement for successful drug development. Compounds outside these limits can still demonstrate success based on their overall profiles and other factors influencingharmacokinetics [18,25,48]. Figure 1 presents the flowchart of the proposed study.

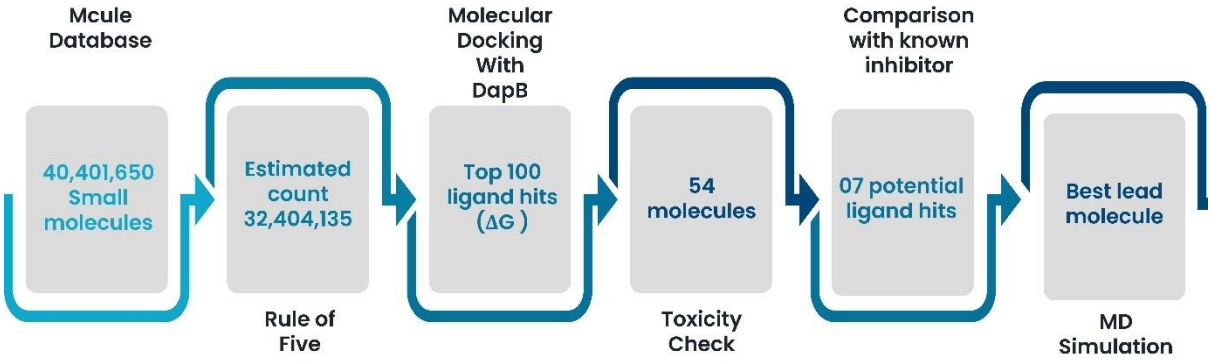

Figure 1. The flowchart for structure-based virtual screening (SBVS) to identify optimal lead molecules targeting DapB in *Mycobacterium tuberculosis*.

3.2. Docking simulation and toxicity assessment of ligand hits.

The MCULE ADV tool was utilized to evaluate the ligand-binding affinities for the screened compounds and the positive control, PDC, by docking them into the DapB binding pocket. The calculated binding free energies (ΔG) for the ligand hits ranged from -9.9 kcal/mol to -8.5 kcal/mol. In comparison, PDC, a known inhibitor, exhibited a ΔG value of -7.5 kcal/mol upon docking into the target protein's binding pocket. PDC engaged with 13 residues through four distinct binding interactions: van der Waals (Vdw), hydrogen bonding (HB), pi-alkyl, and active charge interactions, as illustrated in Figure 2. Following toxicity assessment, only 54 out of 100 ligands were identified as potential drug candidates.

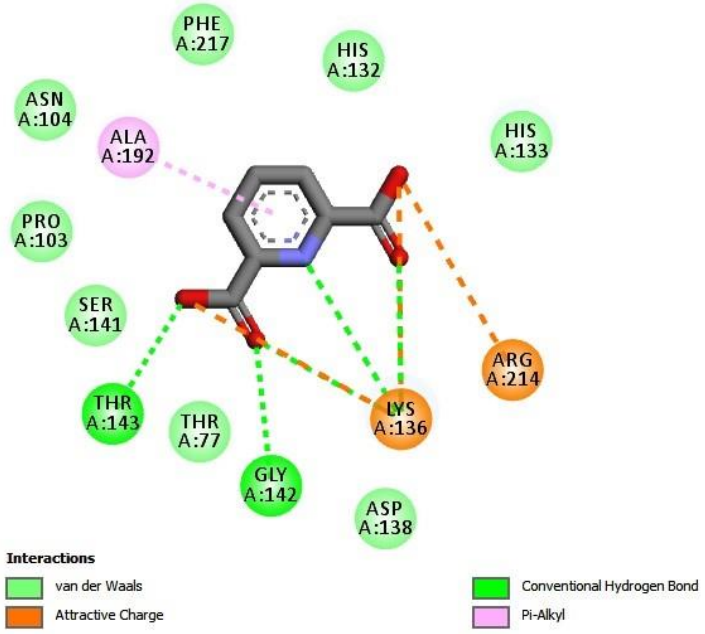

Figure 2. The 2D representation illustrates the intricate molecular interactions between PDC (control) and DapB during protein-ligand docking. The binding between PDC and DapB is characterized by a comprehensive engagement involving van der Waals (vdw) forces, five hydrogen bonds, pi-alkyl interactions, pi-interactions, and active charge interactions.

The selection process focused on ligands with ΔG values equal to or lower than that of PDC (control), interacting residues aligned with the active site in the crystal structure of DapB (PDB: 5TJZ), and demonstrating three or more hydrogen bonds. This rigorous criterion led to identifying 7 of the initial 54 molecules. The computed ΔG values and types of interacting forces in the docking complexes are summarized in Table 1. This stringent approach emphasizes the significance of van der Waals (Vdw), hydrogen bonding (HB), π-alkyl, and

active charge interactions in the ligand-protein binding process. This detailed interaction profile provides insights into the robust binding mechanisms contributing to the stability and specificity of the PDC-DapB complex [18,19,49].

Table 1. Summary of interactions and binding affinities for the top seven hit compounds with active site residues of DapB.

Ligands	DapB	
	ΔG (kcal/mol)	**Types of molecular interactions**
MCULE-2291868853-0-3	-9.2	vdW,7HBs, CHB, pi-pi T-shaped, halogen (fluorine), pi-alkyl
MCULE-3691680594-0-1	-8.5	vdW, 3HBs, alkyl, pi-alkyl, pi-pi Stacked
MCULE-4982806243-0-1	-8.6	vdW, 4HBs, CHB, halogen (fluorine), pi-Alkyl, pi-pi T-shaped
MCULE-7993019654-0-3	-8.5	Vdw, 5HBs, pi-alkyl
MCULE-9296301908-0-1	-9.9	vdW,5HBs, CHB, pi-pi T-shaped, pi-anion, pi-cation, pi-alkyl
MCULE-9496318670-0-1	8.7	Vdw, 4HBs, CHB, alkyl, pi-alkyl, pi-pi T-shaped
MCULE-9929968669-0-44	-8.9	vdW, 3HBs, CHB, Alkyl, pi-alkyl, halogen (fluorine), pi-pi T-shaped
PDC (Control molecule)	-7.5	vdW, HB, attractive charge, pi-alkyl

vdw: van der Waals; HB: Conventional Hydrogen Bond; CHB: Carbon Hydrogen Bond.

3.3. Assessment of human intestinal absorption and blood-brain barrier permeation via BOILED-egg filtration.

As its nomenclature suggests, the model distinguishes between yellow and white regions, representing predictive positions for significant blood-brain barrier (BBB) penetration and human intestinal absorption (HIA) permeation, respectively. Among the seven ligand hits, five—MCULE-2291868853-0-3, MCULE-7993019654-0-3, MCULE-9296301908-0-1, MCULE-9496318670-0-1, and MCULE-9929968669-0-44 exhibited notable HIA permeability, as evidenced by their placement in the white region of the BOILED-Egg model. Additionally, two ligand hits, MCULE-3691680594-0-1 and MCULE-4982806243-0-1, located in the yolk region, suggested their potential for BBB penetration. In contrast, the reference drug PDC displayed significant HIA permeation but lacked BBB penetration.

Figure 3 illustrates the BOILED-egg model predictions for ligands and reference molecules, with blue and red dots indicating P-glycoprotein (P-gp)-positive and P-gp-negative molecules, respectively. This differentiation is crucial, as it signifies that ligands acting as substrates for P-gp are expelled during BBB penetration. In contrast, non-substrate ligands have the potential to traverse the brain membrane [35,50].

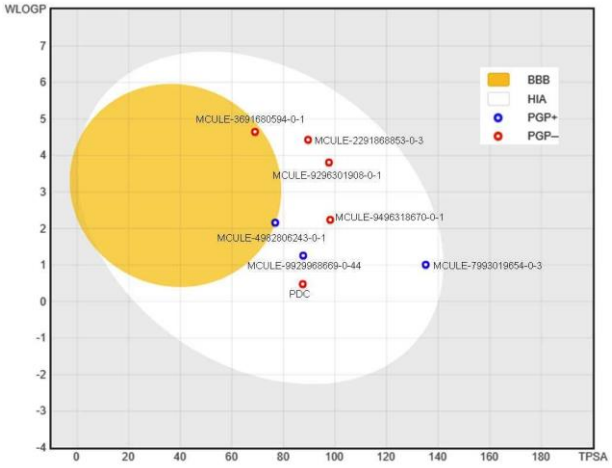

Figure 3. The BOILED-egg model evaluates the passive Human Intestinal Absorption (HIA) permeation and blood-brain barrier (BBB) penetration of ligands, along with control molecules (PDC). Ligand hits and the control molecule in the egg white region indicates HIA permeation, with two specific ligand hits, MCULE-4982806243-0-1 and MCULE-3691680594-0-1, demonstrating potential HIA absorption and BBB permeation. The reference drug, PDC, exhibits significant HIA permeation but lacks BBB permeation.

In this context, the importance of HIA and BBB permeation lies in their impact on drug absorption and distribution within the body. HIA permeation, represented by ligands in the white region, indicates the likelihood of a compound being absorbed through the intestinal wall into the bloodstream, thereby influencing its bioavailability. Conversely, BBB penetration, illustrated by ligands in the yolk region, is essential for drugs targeting the central nervous system because the BBB restricts the entry of many substances into the brain. The BOILED-Egg model, utilizing parameters such as the Total Polar Surface Area (TPSA) on the X-axis and Water-octanol partition coefficient (WLOGP) on the Y-axis, provides insights into these critical pharmacokinetic properties, aiding in the prediction and optimization of drug candidates.

3.4. Comprehensive analysis of drug-likeness of ligands and control molecule.

The Lipinski rule of five served as the primary criterion in the preliminary stage of SBVS. After that, the drug-likeness of the small molecules, with the potential to become promising oral lead compounds, was further assessed using additional parameters, including the Ghose, Veber, Egan, and Muegge criteria. All ligands, with the exception of MCULE-7993019654-0-3, satisfied the drug-likeness rules proposed by Ghose, Veber, Egan, and Muegge [38,51–53]. MCULE-7993019654-0-3, however, exhibited a deviation by surpassing Egan's TPSA threshold of 131.6 $Å^2$. The control drug, PDC, violated Ghose's parameters (MR<40, atoms<20) and Muegge's rule (MW<200) while adhering to the Veber and Egan rules. This underscores the distinctive characteristics of PDC, especially with regard to molecular size and complexity.

A notable observation was the comparison of Bioavailability Scores (BS), where MCULE-9296301908-0-1 and PDC displayed a high BS value of 0.56. The remaining ligands maintained a commendable BS value of 0.55, indicating substantial potential for significant oral absorption (Table 2). A thorough evaluation of diverse drug-likeness parameters highlights the nuanced differences between the ligands and control PDC. This comprehensive approach provides valuable insights into the potential oral lead compounds and aids in refining the selection of candidates for further development.

Table 2. Predicted drug-likeness beyond Lipinski's rule of five for ligands and control drugs.

Molecule	Ghose	Veber	Egan	Muegge	Abbot BS
	Violation(s)				
MCULE-2291868853-0-3	0	0	0	0	0.55
MCULE-3691680594-0-1	0	0	0	0	0.55
MCULE-4982806243-0-1	0	0	0	0	0.55
MCULE-7993019654-0-3	0	0	1 (TPSA>131.6)	0	0.55
MCULE-9296301908-0-1	0	0	0	0	0.56
MCULE-9496318670-0-1	0	0	0	0	0.55
MCULE-9929968669-0-44	0	0	0	0	0.55
PDC (Control molecule)	2 (MR<40, atoms<20)	0	0	1 (MW<200)	0.56

3.5. Analysis of medicinal chemistry parameters.

The medicinal chemistry attributes of various compounds, including PAINS and Brenk alerts, lead-likeness adherence, and synthetic accessibility scores (SS), were thoroughly assessed. The compounds investigated were MCULE-2291868853-0-3, MCULE-4982806243-0-1, MCULE-9496318670-0-1, MCULE-3691680594-0-1, MCULE-7993019654-0-3, MCULE-9296301908-0-1, MCULE-9929968669-0-44, and the control molecule PDC.

MCULE-2291868853-0-3, MCULE-4982806243-0-1, and MCULE-9496318670-0-1 exhibited no PAINS or Brenk alerts and adhered to lead-like rules, displaying SS values of 2.47, 2.81, and 2.97, respectively. Lower SS values suggest easier synthesis, making them excellent drug candidates. MCULE-3691680594-0-1 displayed one Brenk alert (catechol) and one lead-like violation (XLOGP3>3.5). MCULE-7993019654-0-3 and MCULE-9296301908-0-1 violated the lead-likeness rules (MW>350), whereas MCULE-7993019654-0-3 violated the rotor parameters. MCULE-9929968669-0-44 exhibited two lead-like violations (MW>350, rotors >7). PDC, the control molecule, violated the lead-likeness rule with MW<250. The SS values for these compounds ranged from 2.87 to 1.47.

Table 3 summarizes the findings and comprehensively analyzes the medicinal chemistry attributes of the ligands and control drugs. Compounds with zero PAINS and Brenk alerts had structures free of toxicophoric moieties. Adherence to lead-likeness parameters coupled with lower SS values enhances the likelihood of compounds being excellent drug candidates in drug discovery pipelines. Considering each compound's distinct attributes and violations is crucial in selecting potential candidates for wet lab assays [18,54].

Table 3. Analysis of medicinal chemistry parameters for ligands and PDC.

Molecule	PAINS alert	Brenk alert	Lead-likeness violation	Synthetic accessibility
MCULE-2291868853-0-3	0	0	0	2.47
MCULE-3691680594-0-1	0	1 (catechol)	1 (XLOGP3>3.5)	2.87
MCULE-4982806243-0-1	0	0	0	2.81
MCULE-7993019654-0-3	0	0	1 (MW>350)	3.75
MCULE-9296301908-0-1	0	0	1 (MW>350)	2.74
MCULE-9496318670-0-1	0	0	0	2.97
MCULE-9929968669-0-44	0	0	2 (MW>350, Rotors>7)	3.64
PDC (Control molecule)	0	0	1 (MW<250)	1.47

3.6. Hydrogen bond analysis and molecular interactions with DapB target protein.

During the course of investigating interactions with the DapB target protein, various ligands, including the reference drug PDC, exhibited distinct patterns of hydrogen bonding. PDC displayed five conventional hydrogen bonds, MCULE-2291868853-0-3 and MCULE-9296301908-0-1 displayed seven hydrogen bonds, MCULE-3691680594-0-1 displayed three, MCULE-4982806243-0-1 and MCULE-7993019654-0-3 exhibited four, and MCULE-9496318670-0-1 displayed four hydrogen bonds. Notably, all these ligands demonstrated strong binding affinities, as reflected by their more negative ΔG values compared to the control molecule PDC (Table 1).

Seven ligands were selected for further analysis based on the criteria of maximum hydrogen bonds and strong binding affinity relative to the control molecules. Among these, MCULE-2291868853-0-3 and MCULE-9296301908-0-1, which exhibited the highest number of hydrogen bonds and lowest ΔG values, were chosen for in-depth analysis. MCULE-2291868853-0-3 displayed a remarkable ΔG value of -9.2 kcal/mol and engaged with 16 residues through six distinct binding interactions, including van der Waals (vdW), hydrogen bonds (HBs), carbon-hydrogen bond (CHB), pi-pi t-shaped, halogen (fluorine), and pi-alkyl interactions, as illustrated in Figure 4. Similarly, MCULE-9296301908-0-1 exhibited a notable ΔG value of -9.9 kcal/mol and interacted with 21 residues through seven different binding interactions, including van der Waals (Vdw), five hydrogen bonds (5HBs), carbon-hydrogen bonds (CHB), pi-pi t-shaped, pi-anion, pi-cation, and pi-alkyl interactions, as depicted in Figure 5. This detailed analysis provides insights into the diverse molecular interactions, including

hydrogen bonds and other bonding types that contribute to the strong binding affinities of the selected ligands with the DapB target protein.

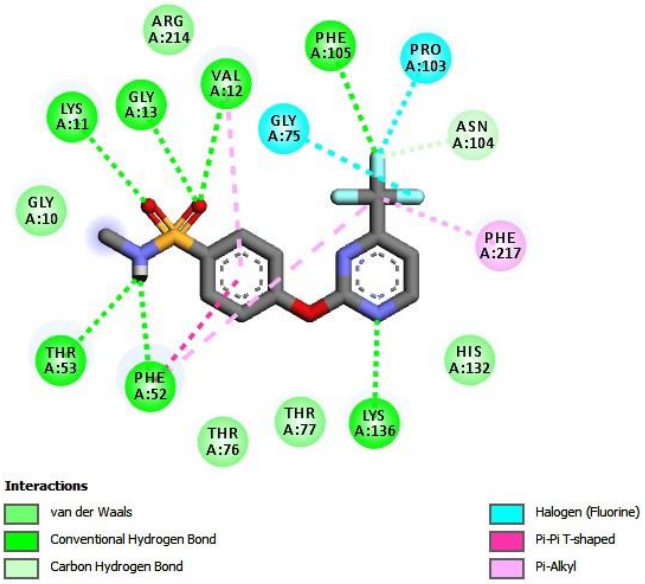

Figure 4. The 2D representation illustrates the intricate molecular interactions between MCULE-2291868853-0-3 and DapB during protein-ligand docking. The binding between MCULE-2291868853-0-3 and DapB is characterized by a comprehensive engagement involving vdW, hbs, CHB, pi-pi t-shaped, halogen (fluorine), and pi-alkyl interactions.

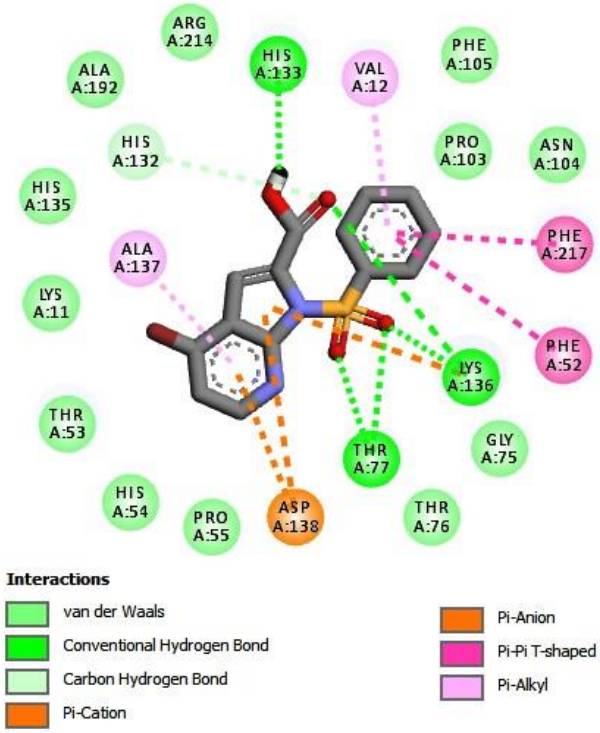

Figure 5. The 2D representation illustrates the intricate molecular interactions between MCULE-9296301908-0-1 and DapB during protein-ligand docking. The binding between MCULE-9296301908-0-1 and DapB is characterized by a comprehensive engagement involving vdW, 5hbs, CHB, pi-pi t-shaped, pi-anion, pi-cation, and pi-alkyl interactions.

3.7. Analysis of docked complex stability through MD simulation.

To assess the stability of the complexes formed by the top two ligand hits, MCULE-2291868853-0-3 (CID: 99771189) (*N*-methyl-4-[4-(trifluoromethyl)pyrimidin-2-

yl]oxybenzenesulfonamide) and MCULE-9296301908-0-1 (CID: 74892780) (1-(benzene sulfonyl)-4-bromopyrrolo[2,3-b]pyridine-2-carboxylic acid), in conjunction with the control molecule PDC (CID: 10367)(2,6-pyridine dicarboxylic acid), we carried out molecular dynamics simulations for a duration of 10 ns using GROMACS software. To scrutinize the stability of molecular interactions within the ligands and protein-docked complexes, we generated graphs depicting the root mean square deviation (RMSD), root mean square fluctuation (RMSF), the radius of gyration (Rg), and hydrogen bonds (HBs) [22,55,56].

3.7.1. Root-mean-square deviation (RMSD) analysis.

The stability of docked complexes was evaluated based on the RMSD metric, which served as a critical parameter. The average RMSD values for the reference inhibitor (turquoise) and the predicted ligand hits MCULE-2291868853-0-3 (maroon) and MCULE-9296301908-0-1 (indigo) when interacting with DapB were determined to be 0.32 nm, 0.45 nm, and 0.23 nm, respectively. The RMSD plot showed that the complex formed by DapB and MCULE-9296301908-0-1 displayed greater stability than that formed by the reference molecule PDC and the other ligand MCULE-2291868853-0-3 with DapB (Figure 6). This suggests that MCULE-9296301908-0-1 is the most promising lead among the ligands and controls PDC regarding stability within the docked complexes.

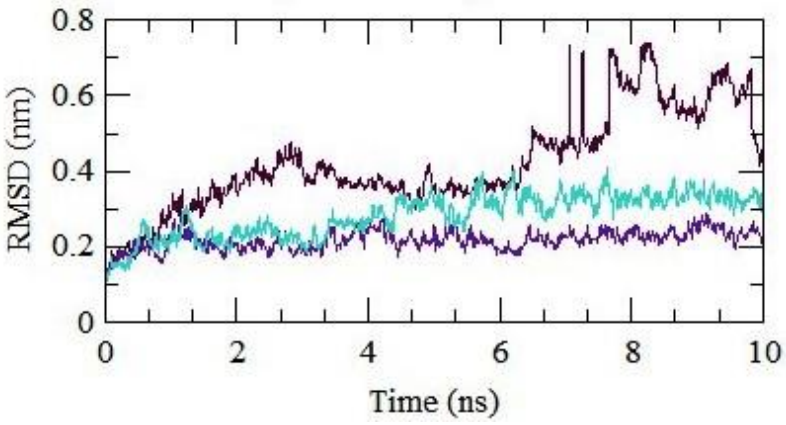

Figure 6. Time-dependent RMSD plot. In the graph, values for the DapB-PDC complex, MCULE-2291868853-0-3 ligand, and MCULE-9296301908-0-1 ligand are represented by turquoise, maroon, and indigo, respectively. The plot illustrates the time-dependent changes in root-mean-square deviation (RMSD) for these entities, providing insights into the structural stability of the complexes over the simulation period.

3.7.2. Root-mean-square fluctuation (RMSF) analysis.

Root mean square fluctuation (RMSF) analysis is a valuable tool for assessing the flexibility of docked complexes, quantifying variations by comparing initial and final fluctuations. The average RMSF values for the DapB-PDC, DapB-MCULE-2291868853-0-3, and DapB-MCULE-9296301908-0-1 complexes were determined to be 0.36 nm, 0.38 nm, and 0.29 nm, respectively. This analysis provides crucial insights into the structural fluctuations exhibited by the docked complexes during molecular dynamics simulations (Figure 7). Notably, the lower RMSF value for the DapB-MCULE-9296301908-0-1 complex suggested reduced structural fluctuations, indicating enhanced stability. Consequently, based on RMSF data, MCULE-9296301908-0-1 emerged as a promising candidate, displaying a more stable interaction than both the DapB-PDC complex and the DapB-MCULE-2291868853-0-3 complex.

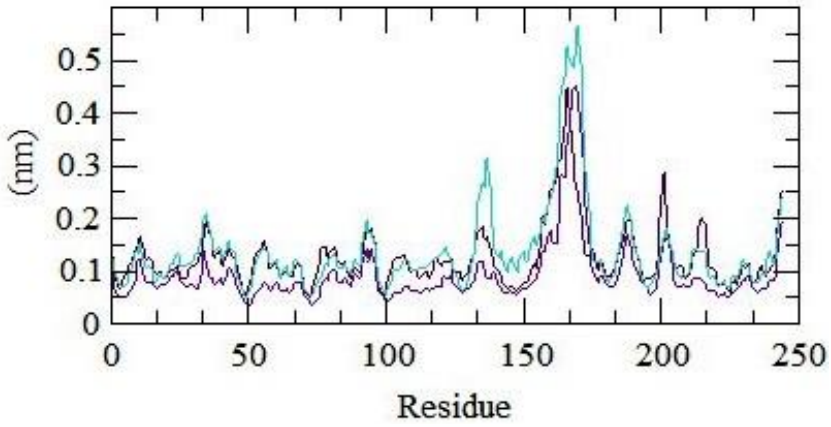

Figure 7. RMSF plot for docked complexes. This graph illustrates the root mean square fluctuation (RMSF) for three distinct complexes: the DapB-PDC complex (turquoise), MCULE-2291868853-0-3 ligand (maroon), and MCULE-9296301908-0-1 (indigo). The plot visually captures the flexibility and variations in structural fluctuations exhibited by each complex over the course of the molecular dynamics simulation.

3.7.3. Radius of gyration (Rg) analysis.

The significance of examining the decreasing trend in the radii of gyration (Rg) with increasing compactness of docked complexes cannot be overstated. The average Rg values for the DapB-PDC complex (turquoise), MCULE-2291868853-0-3 ligand (maroon), and MCULE-9296301908-0-1 (indigo) were determined to be 3.89 nm, 3.78 nm, and 3.79 nm, respectively (Figure 8). This analysis offers critical insights into docked complexes' structural characteristics and compactness during molecular dynamics simulations, providing a solid foundation for further investigations.

Regarding Rg values, both MCULE-2291868853-0-3 and MCULE-9296301908-0-1 exhibited comparable and slightly lower Rg values than those of the DapB-PDC complex. However, the marginal difference suggests similar compactness. Thus, the choice between MCULE-2291868853-0-3 and MCULE-9296301908-0-1 based solely on the Rg values may be inconclusive. Further analyses and comparisons with other parameters are recommended for a comprehensive assessment of ligand performance.

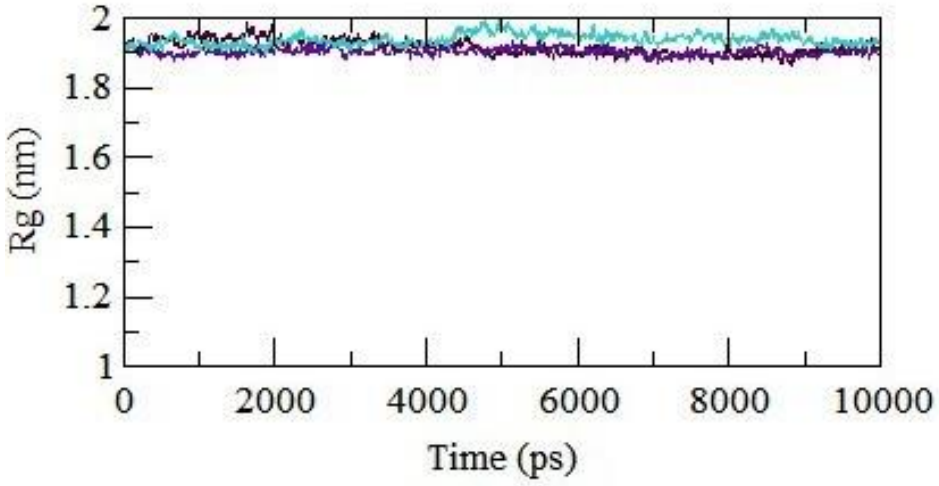

Figure 8. Rg Plot for Docked Complexes. The DapB-PDC complex (turquoise), MCULE-2291868853-0-3 ligand (maroon), and MCULE-9296301908-0-1 (indigo) are depicted in this figure, along with an Rg plot for each of the three distinct complexes. This plot offers a visual representation of each complex's compactness and structural characteristics throughout the molecular dynamics simulation. The plot enables comparative analysis of the overall structural behavior of the different ligands, as each color corresponds to a distinct ligand.

3.7.4. Hydrogen bond formation and deformation analysis of docked complexes during MD simulation.

The hydrogen bond (HB) plot presented in Figure 9 illustrates the number of HB formations, deformations, and stability across the molecular dynamics (MD) simulations for all docked complexes, including the DapB-PDC complex (turquoise), MCULE-2291868853-0-3 ligand (maroon), and MCULE-9296301908-0-1 (indigo). It is worth mentioning that MCULE-2291868853-0-3 initially formed seven HBs upon docking with DapB, but it experienced deformation and remained unstable over the 10ns MD simulation. In contrast, the control molecule PDC and ligand MCULE-9296301908-0-1 exhibited the formation of five stable HBs during their interaction with the target protein throughout the simulation period. This analysis highlights the dynamic behavior of hydrogen bonds within the docked complexes, emphasizing the stability and deformation patterns observed during MD simulations.

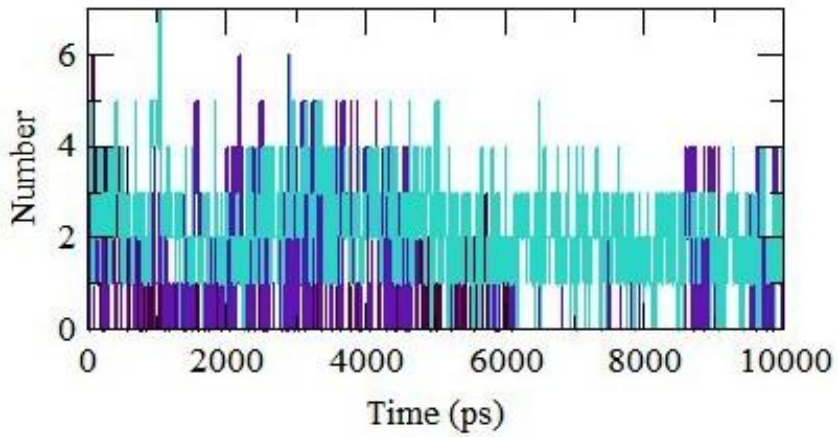

Figure 9. HB Plot for Docked Complexes. This figure illustrates the hydrogen bond (HB) plot for the DapB-PDC complex (turquoise), MCULE-2291868853-0-3 ligand (maroon), and MCULE-9296301908-0-1 (indigo). Each complex is accompanied by an HB plot, providing a visual representation of the hydrogen bond dynamics within the three distinct complexes. The colors correspond to different complexes, facilitating a comparative analysis of their hydrogen bond formation and stability.

3.8. Principal component analysis of docked complexes of ligands and control molecule.

Principal component analysis (PCA) was instrumental in uncovering the prevalent motions and critical conformational alterations present in the trajectories of protein-ligand docking complexes. In the PDC and MCULE-9296301908-0-1, two distinct clusters were observed along the dominant PC1 plane, which exhibited non-periodic conformational changes. In contrast, the variation in MCULE-2291868853-0-3 is relatively low. These findings indicate that PDC (control) displays a greater degree of variation than both ligands, MCULE-9296301908-0-1 and MCULE-2291868853-0-3. The first three principal components collectively accounted for 50.3% (PDC), 28.1% (MCULE-2291868853-0-3), and 56.1% (MCULE-9296301908-0-1) of the overall variance, as evidenced by the eigenvalue rank plot. Specifically, PC1 contributed 31.28% (PDC), 12.52% (MCULE-2291868853-0-3), and 30.46% (MCULE-9296301908-0-1) of the variance, highlighting the distinct conformational behavior of each complex. The dissimilarity in colored dots is attributed to different time samplings, with continuous patterns indicating periodic jumps and gaps signifying energy barriers. The findings from the eigenvalue spectrum analysis and the atomic displacement correlation matrix of the Cα atom coordinates were utilized to unveil these dynamics. A comparison of the results depicted in Figures 10, 11, and 12 for PDC, MCULE-2291868853-

0-3, and MCULE-9296301908-0-1, respectively, shows that MCULE-9296301908-0-1 exhibits more consistent and pronounced conformational changes, suggesting heightened adaptability and dynamic behavior. Thus, MCULE-9296301908-0-1 is a promising candidate with favorable conformational characteristics among the ligands and control PDC.

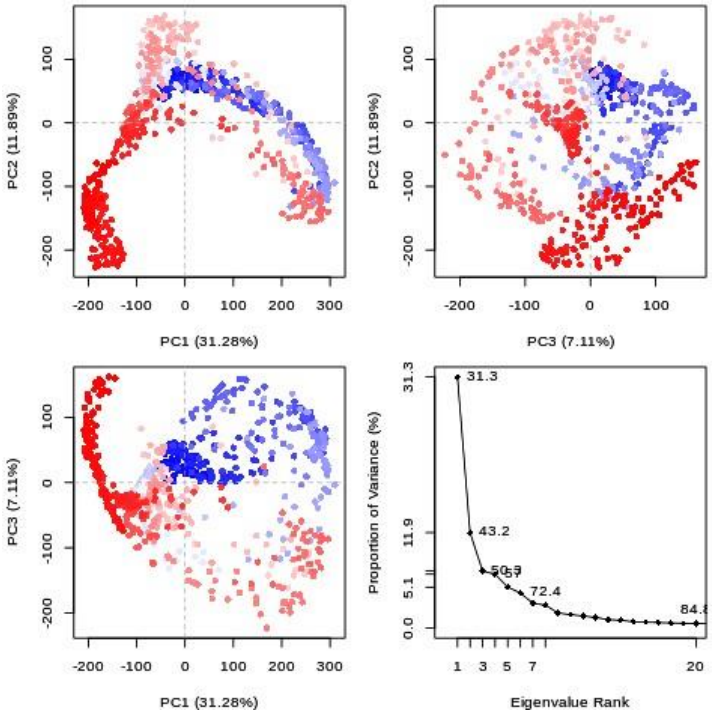

Figure 10. PCA of Cα atoms in DapB backbone motions with control molecule PDC. This figure illustrates the PCA of the Cα atoms, revealing the backbone motions of DapB during the docking process with the control molecule PDC.

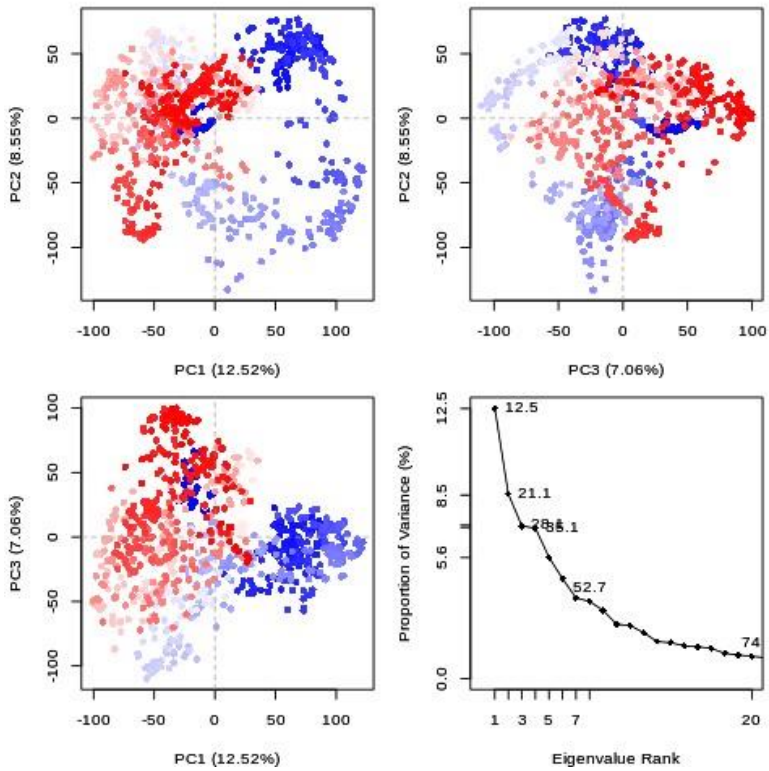

Figure 11. PCA of Cα atoms in DapB backbone motions with MCULE-2291868853-0-3. This figure illustrates the PCA of the Cα atoms, revealing the backbone motions of DapB during the docking process with MCULE-2291868853-0-3.

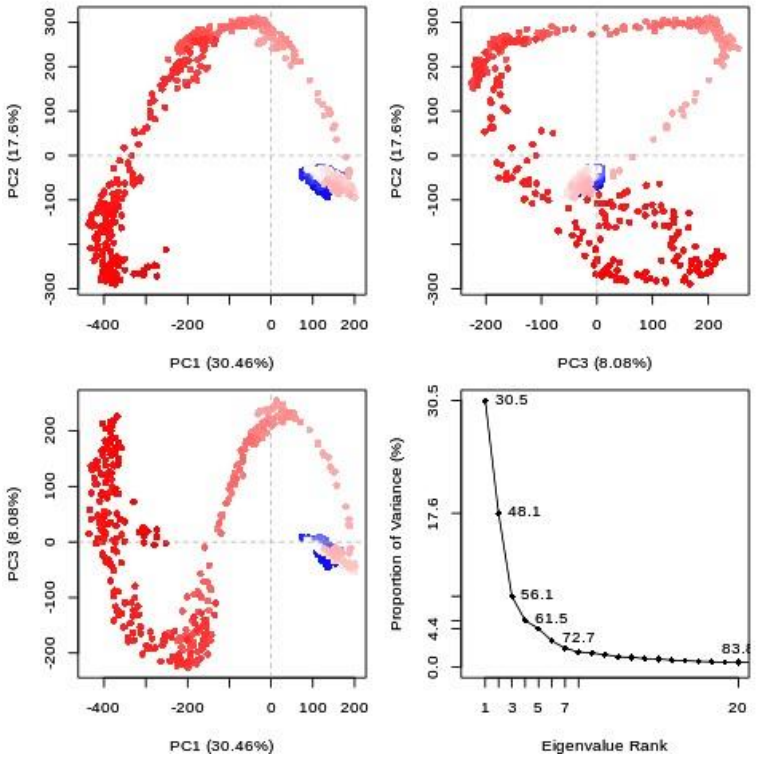

Figure 12. PCA of Cα atoms in DapB backbone motions with MCULE-9296301908-0-1. This figure illustrates the PCA of the Cα atoms, revealing the backbone motions of DapB during the docking process with MCULE-9296301908-0-1.

4. Conclusions

In summary, our extensive analysis encompassing ligand suitability, docking simulations, toxicity assessments, drug-likeness evaluations, and medicinal chemistry parameters, as well as hydrogen bonding and molecular dynamics simulations, identified MCULE-9296301908-0-1 as the most promising lead among the ligands and control PDC. This compound exhibited favorable pharmacokinetic properties, strong binding affinities, reduced structural fluctuations, and enhanced stability during molecular dynamics simulations. Consequently, MCULE-9296301908-0-1 is considered a potential antitubercular agent and a strong candidate for further experimental validation using wet-lab assays.

Funding

No external funding was provided for this research.

Acknowledgments

The authors express their gratitude to Integral University, Lucknow, for providing access to the MD simulation facility utilized in this research.

Conflicts of Interest

The authors have no conflicts of interest to declare.

References

1. Baquero-Artigao, F.; del Rosal, T.; Falcón-Neyra, L.; Ferreras-Antolín, L.; Gómez-Pastrana, D.; Hernanz-Lobo, A.; Méndez-Echevarría, A.; Noguera-Julian, A.; Pascual Sánchez, M.T.; Rodríguez-Molino, P.;

Piñeiro-Pérez, R.; Santiago-García, B.; Soriano-Arandes, A. Actualización del diagnóstico y tratamiento de la tuberculosis. [Update on the diagnosis and treatment of tuberculosis]. *Ann. Pediatr.* **2023**, *98*, 460-469, https://doi.org/10.1016/j.anpedi.2023.03.011.

2. Salari, N.; Kanjoori, A.H.; Hosseinian-Far, A.; Hasheminezhad, R.; Mansouri, K.; Mohammadi, M. Global prevalence of drug-resistant tuberculosis: a systematic review and meta-analysis. *Infect. Dis. Poverty* **2023**, *12*, 57, https://doi.org/10.1186/s40249-023-01107-x.
3. Bacille Calmette–Guérin (BCG) Vaccination and COVID-19. Scientific Brief. *Pediatria i Medycyna Rodzinna* **2020**. https://doi.org/10.15557/PiMR.2020.0025.
4. da Silva, E.H.; Lima, E.; dos Santos, T.R.; Padoveze, M.C. Prevalence and incidence of tuberculosis in health workers: A systematic review of the literature. *Am. J. Infect. Control* **2022**, *50*, 820–827, https://doi.org/10.1016/j.ajic.2022.01.021.
5. Magdalena, D.; Michal, S.; Marta, S.; Magdalena, K.-P.; Anna, P.; Magdalena, G.; Rafał, S. Targeted metabolomics analysis of serum and *Mycobacterium tuberculosis* antigen-stimulated blood cultures of pediatric patients with active and latent tuberculosis. *Sci. Rep.* **2022**, *12*, 4131, https://doi.org/10.1038/s41598-022-08201-4.
6. Bu, Q.; Qiang, R.; Fang, L.; Peng, X.; Zhang, H.; Cheng, H. Global trends in the incidence rates of MDR and XDR tuberculosis: Findings from the global burden of disease study 2019. *Front. Pharmacol.* **2023**, *14*, 1156249, https://doi.org/10.3389/fphar.2023.1156249.
7. Singhal, P.; Dixit, P.; Singh, P.; Jaiswal, I.; Singh, M.; Jain, A. A study on pre-XDR & XDR tuberculosis & their prevalent genotypes in clinical isolates of *Mycobacterium tuberculosis* in north India. *Indian J. Med. Res.* **2016**, *143*, 341-347, https://doi.org/10.4103/0971-5916.182625.
8. Sri, W.; Andi, Z.; Arsin, A.A.; Ansariadi; Sudirman, N.; Masyita, M.; Andi Agus, M. An analysis of risk factors for Multidrug Resistant Tuberculosis (MDR-TB): a hospital-based study. *J. Public Health Dev.* **2023**, *21*, 91–101, https://doi.org/10.55131/jphd/2023/210208.
9. Espinosa-Pereiro, J.; Sánchez-Montalvá, A.; Aznar, M.L.; Espiau, M. MDR Tuberculosis Treatment. *Medicina* **2022**, *58*, 188, https://doi.org/10.3390/medicina58020188.
10. Shaikh, M.S.; Kale, M.A.; Muralidharan, V.; Venkatachalam, T.; Ali, S.S.; Islam, F.; Khan, S.L.; Siddiqui, F.A.; Urmee, H.; Tapadiya, G.G.; Dhawale, S.A.; Ming, L.C.; Ibrahim, I.A.; Alzahrani, A.R.; Sarker, M.M.; Azlina, M.F. The Design, Synthesis, and Evaluation of Diaminopimelic Acid Derivatives as Potential dapF Inhibitors Preventing Lysine Biosynthesis for Antibacterial Activity. *Antibiotics* **2022**, *12*, 47, https://doi.org/10.3390/antibiotics12010047.
11. Liu, N.; Zhang, T.-T.; Rao, Z.-M.; Zhang, W.-G.; Xu, J.-Z. Reconstruction of the Diaminopimelic Acid Pathway to Promote L-lysine Production in *Corynebacterium glutamicum*. *Int. J. Mol. Sci.* **2021**, *22*, 9065, https://doi.org/10.3390/ijms22169065.
12. Sharma, A.; Nadda, A.K.; Shrivastava, R. Chapter 12 - *Myctobacterium tuberculosis* DapA as a target for antitubercular drug design. In Biotechnology of Microbial Enzymes (Second Edition), Brahmachari, G., Ed.; Academic Press: **2023**; pp 279–296, https://doi.org/10.1016/B978-0-443-19059-9.00008-6.
13. Usha, V.; Lloyd, A.J.; Lovering, A.L.; Besra, G.S. Structure and function of *Mycobacterium tuberculosis* meso-diaminopimelic acid (DAP) biosynthetic enzymes. *FEMS Microbiol. Lett.* **2012**, *330*, 10–16, https://doi.org/10.1111/j.1574-6968.2012.02527.x.
14. Pote, S.; Pye, S.E.; Sheahan, T.E.; Gawlicka-Chruszcz, A.; Majorek, K.A.; Chruszcz, M. 4-Hydroxy-tetrahydrodipicolinate reductase from *Neisseria gonorrhoeae* – structure and interactions with coenzymes and substrate analog. *Biochem. Biophys. Res. Commun.* **2018**, *503*, 1993–1999, https://doi.org/10.1016/j.bbrc.2018.07.147.
15. Muduli, S.; Karmakar, S.; Mishra, S. The coordinated action of the enzymes in the L-lysine biosynthetic pathway and how to inhibit it for antibiotic targets. *Biochim. Biophys. Acta - Gen. Subj.* **2023**, *1867*, 130320, https://doi.org/10.1016/j.bbagen.2023.130320.
16. Kiekens, R.; de Koning, R.; Toili, M.E.M.; Angenon, G. The Hidden Potential of High-Throughput RNA-Seq Re-Analysis, a Case Study for DHDPS, Key Enzyme of the Aspartate-Derived Lysine Biosynthesis Pathway and Its Role in Abiotic and Biotic Stress Responses in Soybean. *Plants* **2022**, *11*, 1762, https://doi.org/10.3390/plants11131762.
17. Janowski, R.; Kefala, G.; Weiss, M.S. The structure of dihydrodipicolinate reductase (DapB) from *Mycobacterium tuberculosis* in three crystal forms. *Acta Cryst.* **2010**, *D66*, 61–72, https://doi.org/10.1107/S0907444909043960.

18. Khan, M.K.A.; Alouffi, S.; Ahmad, S. Identifying potential inhibitors of C-X-C motif chemokine ligand10 against vitiligo: structure-based virtual screening, molecular dynamics simulation, and principal component analysis. *J. Biomol. Struct. Dyn.* **2024**, *42*, 8045-8062, https://doi.org/10.1080/07391102.2023.2242952.
19. Khan, M.K.A.; Ahmad, S.; Rabbani, G.; Shahab, U.; Khan, M.S. Target-based virtual screening, computational multiscoring docking and molecular dynamics simulation of small molecules as promising drug candidate affecting kinesin-like protein KIFC1. *Cell Biochem. Funct.* **2022**, *40*, 451–472, https://doi.org/10.1002/cbf.3707.
20. Pote, S.; Kachhap, S.; Mank, N.J.; Daneshian, L.; Klapper, V.; Pye, S.; Arnette, A.K.; Shimizu, L.S.; Borowski, T.; Chruszcz, M. Comparative structural and mechanistic studies of 4-hydroxy-tetrahydrodipicolinate reductases from *Mycobacterium tuberculosis* and *Vibrio vulnificus*. *Biochim. Biophys. Acta - Gen. Subj.* **2021**, *1865*, 129750, https://doi.org/10.1016/j.bbagen.2020.129750.
21. Morris, G.M.; Goodsell, D.S.; Halliday, R.S.; Huey, R.; Hart, W.E.; Belew, R.K.; Olson, A.J. Automated docking using a Lamarckian genetic algorithm and an empirical binding free energy function. *J. Comput. Chem.* **1998**, *19*, 1639–1662, https://doi.org/10.1002/(SICI)1096-987X(19981115)19:14<1639::AID-JCC10>3.0.CO;2-B.
22. Khan, F.I.; Lai, D.; Anwer, R.; Azim, I.; Khan, M.K.A. Identifying novel sphingosine kinase 1 inhibitors as therapeutics against breast cancer. *J. Enzyme Inhib. Med. Chem.* **2020**, *35*, 172–186, https://doi.org/10.1080/14756366.2019.1692828.
23. Ahmad, K.M.K.; Salman, A.; Salman, F.A.-K.; Feras, M.A.-M.; Abdulrahman, M.A.; Jamal, M.A. Computational Exploration of Dibenzo [*a*,*l*] Pyrene Interaction to DNA and its Bases: Possible Implications to Human Health. *Biointerface Res. Appl. Chem.* **2020**, *11*, 11272–11283, https://doi.org/10.33263/BRIAC114.1127211283.
24. Brooks, B.R.; Bruccoleri, R.E.; Olafson, B.D.; States, D.J.; Swaminathan, S.; Karplus, M. CHARMM: A program for macromolecular energy, minimization, and dynamics calculations. *J. Comput. Chem.* **1983**, *4*, 187–217, https://doi.org/10.1002/jcc.540040211.
25. Kiss, R.; Sandor, M.; Szalai, F.A http://Mcule.com: a public web service for drug discovery. *J. Cheminform.* **2012**, *4*, P17, https://doi.org/10.1186/1758-2946-4-S1-P17.
26. Alwabli, A.S. Lead Identification against 3C-like Protease of SARS-CoV-2 Via Target-based Virtual Screening and Molecular Dynamics Simulation. *J. Young Pharm.* **2022**, *14*, 179–186, https://doi.org/10.5530/jyp.2022.14.34.
27. Lu, S.; Liao, X.; Lu, W.; Zhang, L.; Na, K.; Li, X.; Guo, X. L-Alanine promotes anti-infectious properties of *Bacillus subtilis* S-2 spores via the germination receptor gerAA. *Probiotics Antimicrob. Proteins* **2024**, *16*, 1399-1410, https://doi.org/10.1007/s12602-023-10121-2.
28. Macchiagodena, M.; Pagliai, M.; Procacci, P. Characterization of the non-covalent interaction between the PF-07321332 inhibitor and the SARS-CoV-2 main protease. *J. Mol. Graph. Model.* **2022**, *110*, 108042, https://doi.org/10.1016/j.jmgm.2021.108042.
29. Narayanan, N.; Nair, D.T. Ritonavir may inhibit exoribonuclease activity of nsp14 from the SARS-CoV-2 virus and potentiate the activity of chain terminating drugs. *Int. J. Biol. Macromol.* **2021**, *168*, 272–278, https://doi.org/10.1016/j.ijbiomac.2020.12.038.
30. Dayer, M.R.; Taleb-Gassabi, S.; Dayer, M.S. Lopinavir; A Potent Drug against Coronavirus Infection: Insight from Molecular Docking Study. *Arch. Clin. Infect. Dis.* **2017**, *12*, e13823, https://doi.org/10.5812/archcid.13823.
31. Trott, O.; Olson, A.J. AutoDock Vina: Improving the speed and accuracy of docking with a new scoring function, efficient optimization, and multithreading. *J. Comput. Chem.* **2010**, *31*, 455-461, https://doi.org/10.1002%2Fjcc.21334.
32. Nehal, M.; Khatoon, J.; Akhtar, S.; Khan, M.K.A. Computational insights into inhibiting EphA2: Integrating structure-based virtual screening, docking, and molecular dynamics simulations for small molecule discovery. *Cellular and Molecular Biology.* **2024**, *70(8)*, 16–31. https://doi.org/10.14715/cmb/2024.70.8.3
33. Khan, M.K.A.; Akhtar, S.; Arif, J.M. Development of In Silico Protocols to Predict Structural Insights into the Metabolic Activation Pathways of Xenobiotics. *Interdiscip. Sci. Comput. Life Sci.* **2018**, *10*, 329–345, https://doi.org/10.1007/s12539-017-0237-4.
34. Khan, M.K.A.; Akhtar, S.; Arif, J.M. Structural Insight into the Mechanism of Dibenzo[*a*,*l*]pyrene and benzo[*a*]pyrene-Mediated Cell Proliferation Using Molecular Docking Simulations. *Interdiscip. Sci. Comput. Life Sci.* **2018**, *10*, 653–673, https://doi.org/10.1007/s12539-017-0226-7.

35. Daina, A.; Michielin, O.; Zoete, V. SwissADME: a free web tool to evaluate pharmacokinetics, drug-likeness and medicinal chemistry friendliness of small molecules. *Sci. Rep.* **2017**, *7*, 42717, https://doi.org/10.1038/srep42717.
36. Attique, S.A.; Hassan, M.; Usman, M.; Atif, R.M.; Mahboob, S.; Al-Ghanim, K.A.; Bilal, M.; Nawaz, M.Z. A Molecular Docking Approach to Evaluate the Pharmacological Properties of Natural and Synthetic Treatment Candidates for Use against Hypertension. *Int. J. Environ. Res. Public Health* **2019**, *16*, 923, https://doi.org/10.3390/ijerph16060923.
37. Egan, W.J.; Merz, K.M.; Baldwin, J.J. Prediction of Drug Absorption Using Multivariate Statistics. *J. Med. Chem.* **2000**, *43*, 3867–3877, https://doi.org/10.1021/jm000292e.
38. Egan, W.J.; Lauri, G. Prediction of intestinal permeability. *Adv. Drug Deliv. Rev.* **2002**, *54*, 273–289, https://doi.org/10.1016/S0169-409X(02)00004-2.
39. Baell, J.B.; Holloway, G.A. New Substructure Filters for Removal of Pan Assay Interference Compounds (PAINS) from Screening Libraries and for Their Exclusion in Bioassays. *J. Med. Chem.* **2010**, *53*, 2719–2740, https://doi.org/10.1021/jm901137j.
40. Brenk, R.; Schipani, A.; James, D.; Krasowski, A.; Gilbert, I.H.; Frearson, J.; Wyatt, P.G. Lessons Learnt from Assembling Screening Libraries for Drug Discovery for Neglected Diseases. *ChemMedChem* **2008**, *3*, 435–444, https://doi.org/10.1002/cmdc.200700139.
41. Van Der Spoel, D.; Lindahl, E.; Hess, B.; Groenhof, G.; Mark, A.E.; Berendsen, H.J.C. GROMACS: Fast, flexible, and free. *J. Comput. Chem.* **2005**, *26*, 1701–1718, https://doi.org/10.1002/jcc.20291.
42. Vanommeslaeghe, K.; MacKerell Jr., A.D. Automation of the CHARMM General Force Field (CGenFF) I: Bond Perception and Atom Typing. *J. Chem. Inf. Model* **2012**, *52*, 3144–3154, https://doi.org/10.1021/ci300363c.
43. Vanommeslaeghe, K.; Hatcher, E.; Acharya, C.; Kundu, S.; Zhong, S.; Shim, J.; Darian, E.; Guvench, O.; Lopes, P.; Vorobyov, I.; Mackerell Jr, A.D. CHARMM general force field: A force field for drug-like molecules compatible with the CHARMM all-atom additive biological force fields. *J. Comput. Chem.* **2010**, *31*, 671–690, https://doi.org/10.1002/jcc.21367.
44. Petersen, H.G. Accuracy and efficiency of the particle mesh Ewald method. *J. Chem. Phys.* **1995**, *103*, 3668–3679, https://doi.org/10.1063/1.470043.
45. Stenberg, S.; Stenqvist, B. An Exact Ewald Summation Method in Theory and Practice. *J. Phys. Chem. A* **2020**, *124*, 3943–3946, https://doi.org/10.1021/acs.jpca.0c01684.
46. Fischer, N.M.; van Maaren, P.J.; Ditz, J.C.; Yildirim, A.; van der Spoel, D. Properties of Organic Liquids when Simulated with Long-Range Lennard-Jones Interactions. *J. Chem. Theory Comput.* **2015**, *11*, 2938–2944, https://doi.org/10.1021/acs.jctc.5b00190.
47. Dhanasekaran, S.; Pushparaj Selvadoss, P.; Sundar Manoharan, S.; Jeyabalan, S.; Devi Rajeswari, V. Revealing anti-fungal potential of plant-derived bioactive therapeutics in targeting secreted aspartyl proteinase (SAP) of *Candida albicans*: a molecular dynamics approach. *J. Biomol. Struct. Dyn.* **2024**, *42*, 710-724, https://doi.org/10.1080/07391102.2023.2196703.
48. Lipinski, C.A. Lead- and drug-like compounds: the rule-of-five revolution. *Drug Discov. Today Technol.* **2004**, *1*, 337–341, https://doi.org/10.1016/j.ddtec.2004.11.007.
49. Akhtar, S.; Khan, M.K.A.; Arif, J.M. Evaluation and Elucidation Studies of Natural Aglycones for Anticancer Potential Using Apoptosis-Related Markers: An In Silico Study. *Interdiscip. Sci. Comput. Life Sci.* **2018**, *10*, 297–310, https://doi.org/10.1007/s12539-016-0191-6.
50. Walker, G.; Franson, A.F.; Pai, M.; Ravi, K.; Roberts, H.; Schepers, A.; Koschmann, C.J.; Marini, B.L. Predicting CNS penetration of precision medicine therapies in oncology: A comparison of the CNS TAP tool and the BOILED-Egg computational model. *J. Clin. Oncol.* **2022**, *40*, 2062, https://doi.org/10.1200/JCO.2022.40.16_suppl.2062.
51. Ghose, A.K.; Viswanadhan, V.N.; Wendoloski, J.J. A Knowledge-Based Approach in Designing Combinatorial or Medicinal Chemistry Libraries for Drug Discovery. 1. A Qualitative and Quantitative Characterization of Known Drug Databases. *J. Comb. Chem.* **1999**, *1*, 55–68, https://doi.org/10.1021/cc9800071.
52. Veber, D.F.; Johnson, S.R.; Cheng, H.-Y.; Smith, B.R.; Ward, K.W.; Kopple, K.D. Molecular Properties That Influence the Oral Bioavailability of Drug Candidates. *J. Med. Chem.* **2002**, *45*, 2615–2623, https://doi.org/10.1021/jm020017n.
53. Muegge, I.; Heald, S.L.; Brittelli, D. Simple Selection Criteria for Drug-like Chemical Matter. *J. Med. Chem.* **2001**, *44*, 1841–1846, https://doi.org/10.1021/jm015507e.

54. Lipinski, CA. Drug-like properties and the causes of poor solubility and poor permeability. *J Pharmacol Toxicol Methods*. ***2000***;*44(1)*, 235-249. doi:10.1016/s1056-8719(00)00107-6
55. Ali, S.; Khan, F.I.; Mohammad, T.; Lan, D.; Hassan, M.I.; Wang, Y. Identification and Evaluation of Inhibitors of Lipase from *Malassezia restricta* using Virtual High-Throughput Screening and Molecular Dynamics Studies. *Int. J. Mol. Sci.* **2019**, *20*, 884, https://doi.org/10.3390/ijms20040884.
56. Kuzmanic, A.; Zagrovic, B. Determination of Ensemble-Average Pairwise Root Mean-Square Deviation from Experimental B-Factors. *Biophys. J.* **2010**, *98*, 861–871, https://doi.org/10.1016/j.bpj.2009.11.011.